Cold Remote Nitrogen Plasma Polymerization from 1.1.3.3-Tetramethyldisiloxane–Oxygen Mixture

F. CALLEBERT,[1] Ph. SUPIOT,[1] K. ASFARDJANI,[1] O. DESSAUX,[1] P. GOUDMAND,[1] P. DHAMELINCOURT,[2] and J. LAUREYNS[2]

[1]Laboratoire de Physicochimie, de l'Energétique et des Plasmas, LPCEP, Université des Sciences et des Technologies de Lille, 59655 Villeneuve d'Ascq, France, and [2]Laboratoire de Spectrochimie Infrarouge et Raman, LASIR, CNRS UPR 2631L, Université des Sciences et des Technologies de Lille, 59655 Villeneuve d'Ascq, France

SYNOPSIS

Cold remote nitrogen plasma (CRNP) selectively reacts with silane-terminated organosiloxane compounds such as 1.1.3.3-tetramethyldisiloxane to give polymeric layers. Deposition rate measurements, FT-IR and Raman spectroscopy were performed. The chemical composition of the deposited film is closely dependent on the reactive gas composition and its flowing conditions. An original effect of dioxygen addition in the nonionic reactive media is pointed out: dioxygen addition leads to a fast and highly hydrocarbonated polymer formation with a nitrogen fixation in a silazane structure. Polymerization is described by a model where $\equiv Si-O^{\bullet}$ type of radicals are the critical reactant. A global mechanism is proposed involving active species of the CRNP in initiation step of hydrogen abstraction and the nitrogen triplet state molecule $N_2(A\ ^3\Sigma)$ in methyl abstraction on $\equiv Si^{\bullet}$ type of free radical. Dioxygen adjunction appears to limit the methyl abstraction steps. The efficient direct oxygen reaction on free radicals leads to an increase of the $\equiv Si-O^{\bullet}$ radical density and, consequently of the average length of the growing polymeric fragments. Nitrogen fixation, involving oxygenated species, is discussed. Under defined conditions, a highly hydrophobic polymeric film is obtained with a volumic mass of 1.34 g/cm^3 and a deposition rate of about 12 mg/cm^2 h corresponding to a growth rate of 200 Å/s. © 1994 John Wiley & Sons, Inc.

INTRODUCTION

Plasma-enhanced chemical vapor deposition (PECVD) under pressure between 10^{-2} and 10^{-1} hPa have been subjected to numerous previous works.[1] Primary physicochemical processes in discharge involve electronic excitation and ionization of molecules by rapid electrons and high-energy UV photons. They lead to free-radicals formation, and their homogeneous and heterogeneous phases recombination involve the growth of a polymeric film deposit.

This PECVD process is not selective for the polymerization precursor gas;[2-4] it has a poor deposition rate[5] by the fact of etching induced by electron and ion bombardment phenomena. Under such conditions, the deposition rate does not exceed 0.6 mg/cm^2 h for organosiloxane compounds.[6]

We have developed an other trend for plasma deposition induced by cold remote nitrogen plasma[7] (CRNP). Specific industrial aspects of those plasma polymers have been protected by an international patent application.[8] This reactive and energetic medium is obtained by flowing extraction of excited species from a microwave discharge under a pressure ranging from 3 to 20 hPa. Its reactivity is mainly due to long-lived particles: ground state atoms $N(^4S)$, metastable triplet state $N_2(A\ ^3\Sigma_u^+)$ and ground-state vibrationally excited $N_2(X\ ^1\Sigma_g^+)_v$ molecules. This highly thermodynamic nonequilibrium medium does not contain any electrons or photons with an energy sufficient to break chemical bonds. It can be obtained in large volumes.[9]

Journal of Applied Polymer Science, Vol. 52, 1595–1606 (1994)
 CCC 0021-8995/94/111595-12

Organosiloxane compound polymerization is described in the present study. Their polymerizations by PECVD have been studied in numerous previous works.[6,10-16]

CRNP offers the following advantages, as discussed in this study:

1. No etching of the deposit by reactive species, leading to a higher deposition rate.
2. The low viscosity of the nonionic reactive media offers a good deposition homogeneity even on complex surfaces.
3. CRNP treatment of the target surface increases adhesion of the deposited layer.

We will expose successively:

1. Observations and experimental results on the deposition rate versus the nature of the organosiloxane compound (M) and the reactive gas (RG) composition where RG is the mixture M + (Ar or O_2). The important role of the ground-state dioxygen molecule is pointed out.
2. Results concerning the influence of the RG composition on the physicochemical characteristic properties of the deposited layer.

EXPERIMENTAL

General Device

Figure 1 shows the experimental setup of a CRNP assisted deposition reactor. Nitrogen is introduced, under a pressure (p) of 4.8 hPa at a flow rate (ϕ_{N_2}) of 1.8 slpm in a Pyrex discharge tube of 33 mm outer diameter. Discharge plasma (CRNP precursor) excitation is created either with a 433-MHz excitation using a Dupret-Sommer[8] coaxial coupling device or with a Moreau-type rectangular coupling device[17] at 2450 MHz. The discharge useful power (P_u) is, in the co-current reactor, 300 W at 433 MHz and 700 W at 2450 MHz in the countercurrent reactor.

The gas containing excited species is extracted from the discharge zone by a primary pump, Alcatel 33 m^3/h. RG is injected in the reaction chamber, 1.5 m downstream of the discharge in order to avoid retrodiffusion toward the discharge. Photoluminescence effects from the intense glow of the discharge are removed by a light trap before the reaction chamber. Under those conditions, the density of the nitrogen atoms, estimated by NO titration, is about 1.10^{14} atoms/cm^3.

Nitrogen and argon are Air Liquide "U" grade, oxygen is Air Liquide "C" grade. The pressure of the reactive media is controlled by an Edwards PRH 10 Pirani type vacuum gauge. The flow rates of gases are regulated by Alphagaz RDM 280 mass flow regulators (MFR).

Monomers are 1.1.3.3-tetramethyldisiloxane 97% (TMDS) and hexamethyldisiloxane 97% (HMDS) purchased from Aldrich Chemical Co. Monomer flow rate can be regulated from 0 to 160 sccm. Deposits are obtained on 5 cm^2 glossy aluminum disks and analyzed by a Perkin-Elmer FT-IR 1600 spectrometer with a 15° specular reflexion device and by a Dilor XY Raman microspectroscope. The Raman exciting source is the green line at 514.5 nm of an ionized argon laser. The deposition rate (V_D) is

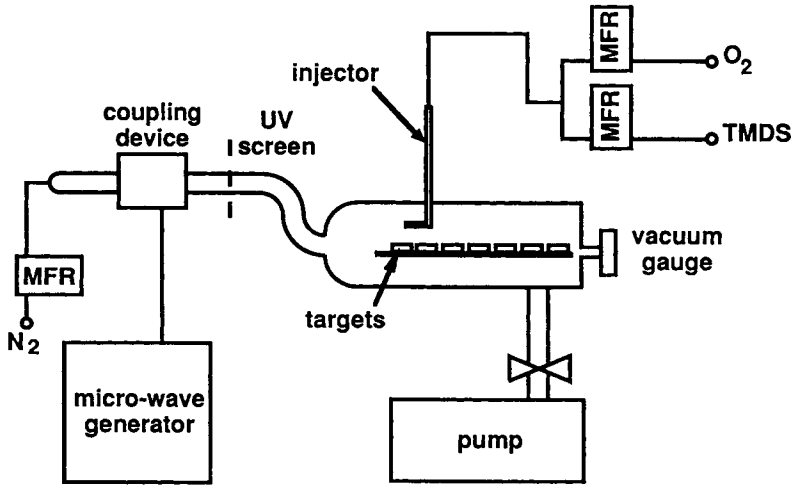

Figure 1 Experimental setup: countercurrent reactor.

evaluated by gravimetric determination and the thickness by a Alpha-Step piezoelectric stylus. Surface energy is evaluated by water drop contact angle measurement. The CRNP/RG reaction is followed by a Jobin-Yvon THR 1000 UV-VIS spectrometer.

Influence of Reactor Geometry

This study has pointed out the most important influence of the reactive gas mixture on physicochemical properties, kinetic and localization of the deposit.

1. A co-current reactor where the target is located normally to the flow, described in a previous study.[18]
2. A countercurrent reactor where the target lays in the axis of the main gas flow (Fig. 1). A coplanar target network is then used to determine the precise location of the deposit.

RESULTS

General Considerations

TMDS or HMDS injection in the CRNP involves a lilas chemiluminescence. The gas phase reaction of TMDS has been previously described.[18] The adjunction of argon to TMDS, at a flow rate from 0 to 150 sccm, does not modify the chemiluminescence; but, under the same conditions, dioxygen adjunction to TMDS leads to an intensification and a modification of volumic chemiluminescence phenomena.

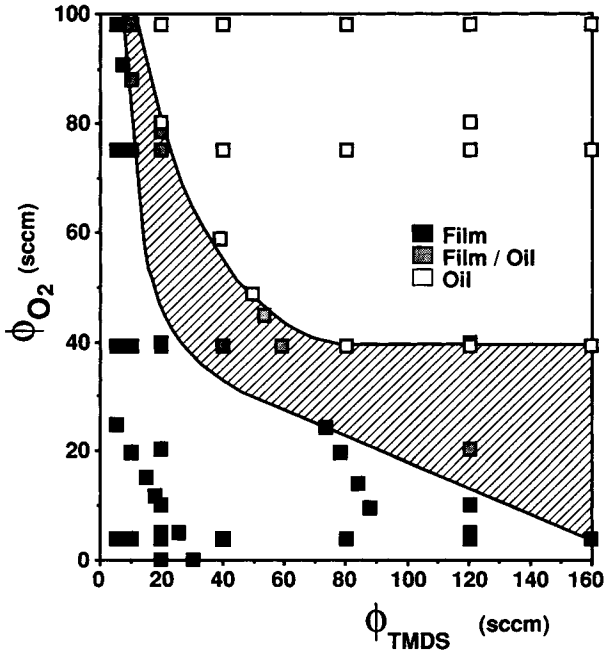

Figure 2 Co-current reactor: film and oil region.

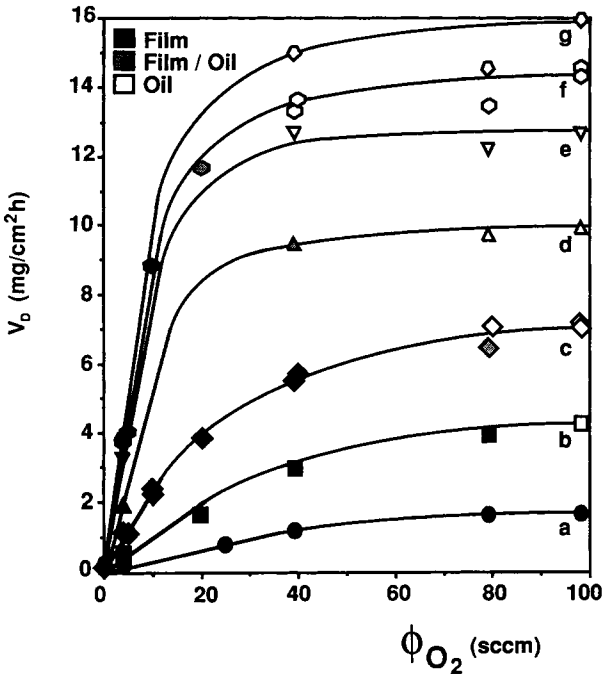

Figure 3 Co-current reactor: V_D at fixed ϕ_{TMDS}: (a) 5; (b) 10; (c) 20; (d) 40; (e) 80; (f) 120; (g) 160 (sccm) (P_u = 300 W; p = 4.8 hPa; ϕ_{N_2} = 1.8 slpm).

No significant deposit is observed by HMDS injection in the CRNP, even with a vector gas. Furthermore, TMDS gives a deposit with a high deposition rate. V_D increases with dioxygen addition.

We will study the influence of TMDS–O_2 mixture on V_D, the FT-IR, and Raman spectroscopy of the deposit.

V_D in the Co-current Reactor

In order to obtain homogeneous deposits, the target is located at 20 cm of the injector inlet. An adhesive hard film as well as an oily deposit can be obtained by variation of the O_2 flow rate in the reactive gas.

Figure 2 shows the oily and film region versus oxygen and monomer flow rates (ϕ_{O_2} and ϕ_{TMDS}, respectively). A transition zone appears between the two types of deposits.

Figure 3 shows that, at constant ϕ_{TMDS}, V_D is enhanced when ϕ_{O_2} increases and allows us to distinguish the oily deposit from the film deposit.

The same result is given in Figure 4 where ϕ_{O_2} is kept constant. Figure 5 represent the influence of

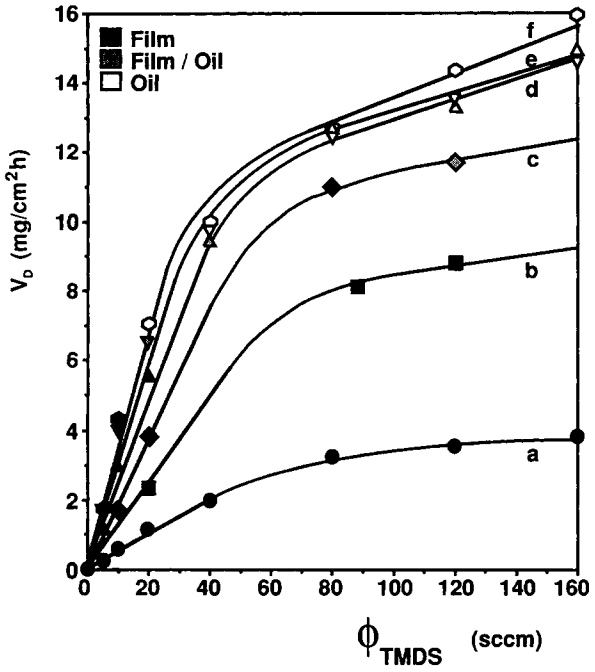

Figure 4 Co-current reactor: V_D at fixed ϕ_{O_2}: (a) 4; (b) 10; (c) 20; (d) 40; (e) 75; (f) 98 (sccm) (P_u = 300 W; p = 4.8 hPa; ϕ_{N_2} = 1.8 slpm).

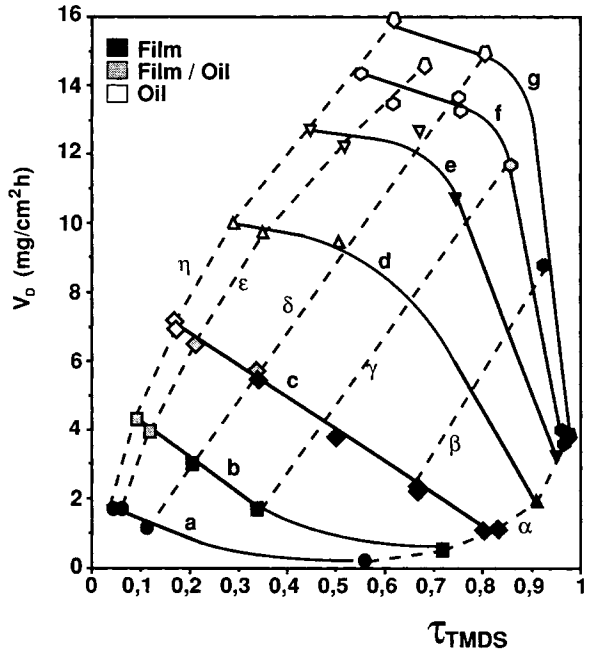

Figure 5 Co-current reactor: V_D vs. stoichiometric parameter τ_{TMDS}. (P_u = 300 W; p = 4.8 hPa; ϕ_{N_2} = 1.8 slpm): Solid lines: ϕ_{TMDS} = (a) 5; (b) 10; (c) 20; (d) 40; (e) 80; (f) 120; (g) 160 (sccm). Dashed lines: ϕ_{O_2}: (α) 4; (β) 10; (γ) 20; (δ) 40; (ε) 75; (η) 98 (sccm).

the stoichiometric parameter τ_{TMDS} on V_D for various ϕ_{TMDS} and ϕ_{O_2} where τ_{TMDS} is given by

$$\tau_{TMDS} = \frac{\phi_{TMDS}}{\phi_{TMDS} + \phi_{O_2}}$$

Under specific conditions, a hard film deposit can be obtained at a V_D of 12 mg/cm² h. Thickness measurements, by the threshold method, give V_D range of 200 Å/s, with a corresponding volumic mass of 1.34 g/cm³.

V_D in the Countercurrent Reactor

In such geometry, a point and a stopping area of gaseous flows appear. In this area, the flows are locally unstable, leading to a high heterogeneity of the deposit.

V_D is then dependent on the spatial location of the target from the injector inlet. V_D reaches a maximum value in the stopping area and rapidly decreases downstream of the injector inlet (Fig. 6). Water drop contact angle measurements show high values ($\theta_w > 160°$) on the deposit obtained in the stopping area and lower, similar to those obtained on silica ($\theta_w \sim 50°$), on the deposit obtained downstream of the injection zone.

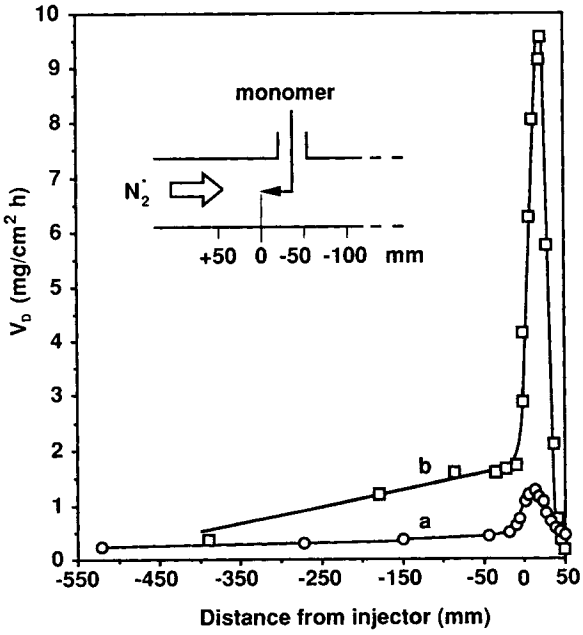

Figure 6 Countercurrent reactor: Longitudinal dependence of V_D (a) ϕ_{TMDS} = 120 sccm; (b) ϕ_{TMDS} = 120 sccm, ϕ_{O_2} = 20 sccm (P_u = 700 W; p = 4.8 hPa; ϕ_{N_2} = 1.8 slpm).

SPECTROSCOPIC RESULTS

FT-IR and Raman Analysis of Plasma Polymers in the Co-current Reactor

Chemical composition is closely dependent on τ_{TMDS}. Figure 7 shows FT-IR 15° specular reflexion spectra of deposits without dioxygen addition. The increase of ϕ_{TMDS} does not affect spectral characteristics: a sharp band assigned to the CH_3 symetric bending mode strongly coupled with Si—C stretching and Si—C—H bending motions[19] appears at 1270 cm^{-1} and is characteristic of $Si(CH_3)_1$ in a polysiloxane structure. Correlatively, the band observed at 800 cm^{-1} is characteristic of a Si—C—H bending motion. The polymeric structure is evidenced by a broad band appearing between 1000 and 1150 cm^{-1}, which is assigned to the Si—O—Si stretching mode.[20]

At constant ϕ_{O_2} (4 sccm) and for an increase of ϕ_{TMDS}, a progressive intensification of the bands appearing in the 1410–1450 cm^{-1} range is observed. These bands are characteristic of the bending modes of the methyl groups (Fig. 8). The bands observed at 2125 and 2215 cm^{-1} are characteristic of Si—H stretching modes. The increase of the intensity of this last band with ϕ_{TMDS} is indicative of the modification of the environment of the silicon atom linked to an hydrogen atom. NH group is evidenced by its vibration band at 3380 and 945 cm^{-1}. A complex broad spectroscopic structure between 1170 and 1000 cm^{-1} can be explained by the overlapping of the absorption of Si—O—Si and Si—NH—Si groups. This structure is accompanied, for high ϕ_{TMDS}, by an increase of Si—NH—Si structure, and a weakening of Si—O—Si absorption.

When dioxygen concentration increases in the reactive media at fixed ϕ_{TMDS} (20 sccm) (Fig. 9), an absorption band at 3400 cm^{-1} is observed, which broadens and gradually transforms into a large band in the range of 3400–3300 cm^{-1}. This one is assigned to an hydrogen bonded Si—OH group. Simultaneously, the band corresponding to the antisymmetric stretching mode of the methyl group sharpens and the band corresponding to the symmetric bending of the methyl group, strongly coupled to Si—C stretching and Si—C—H bending motions, appear respectively at 1260 and 1250 cm^{-1} for $Si(CH_3)_2$ and $Si(CH_3)_3$.

Oily deposit FT-IR spectrum [Fig. 9(f)] does not show any evolution of the global structure of the polymer versus ϕ_{TMDS} or ϕ_{O_2}. A very intense absorption of Si—OH and Si—NH groups, a sharp band at 1250 cm^{-1}, previously assigned to a Si—C stretching and CH_3 bending mode in $Si(CH_3)_3$, a band at 2130 cm^{-1} assigned to SiH motions and a nonassigned broad band at 1660–1680 cm^{-1} are the main characteristics of this deposit. The last band is systematically evidenced in CRNP assisted polymerization of silazanes.

Those spectroscopic results fit well with the micro-Raman spectrometry. Figure 10 shows the Raman spectra of fused silica [Fig. 10(a)], deposit

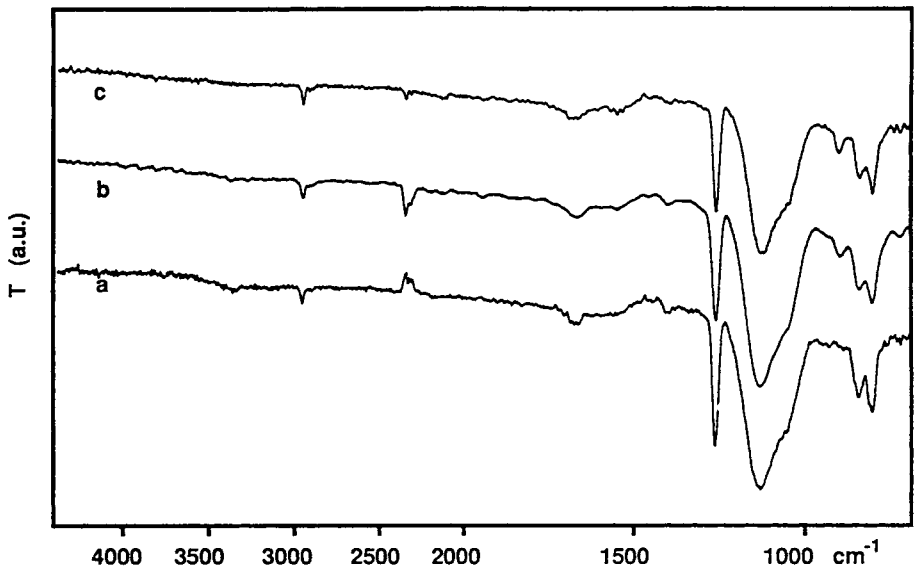

Figure 7 Co-current reactor: FT-IR spectra of deposit (TMDS without O_2): ϕ_{TMDS}: (a) 20; (b) 98; (c) 160 (sccm) (P_u = 300 W; p = 4.8 hPa; ϕ_{N_2} = 1.8 slpm).

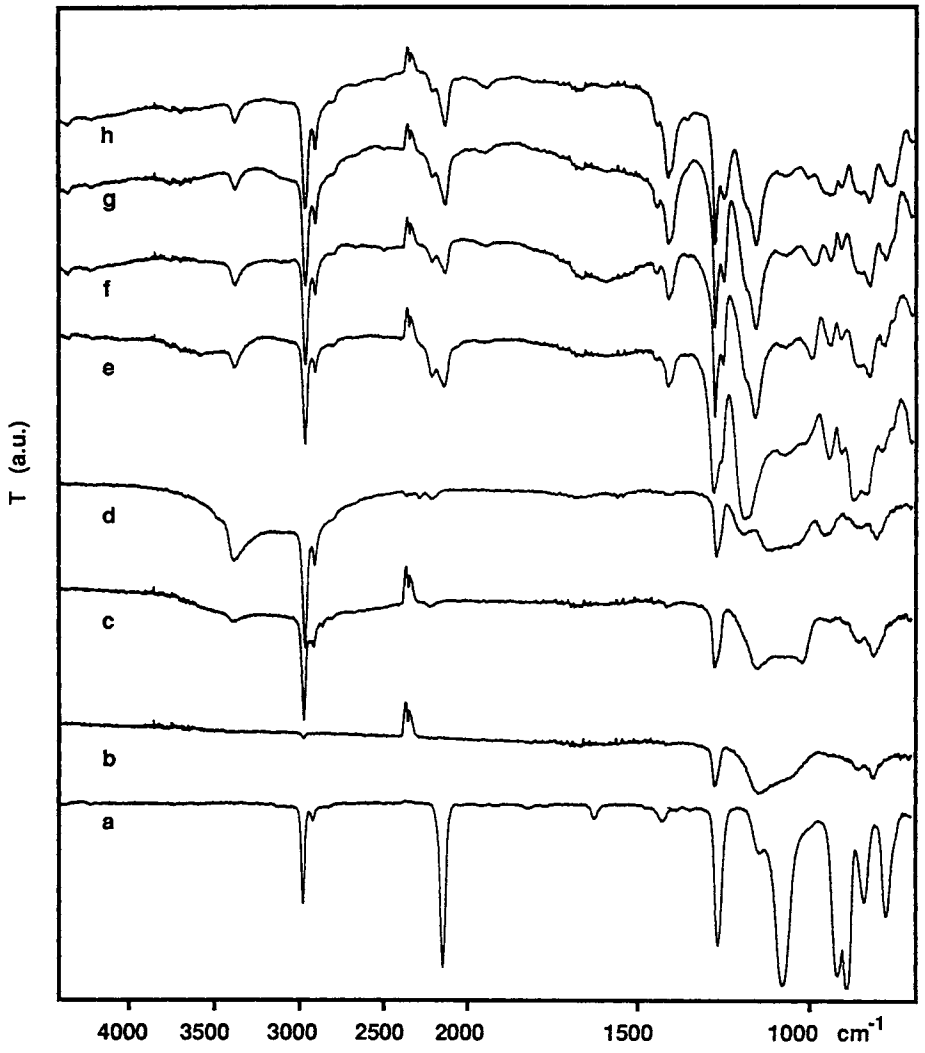

Figure 8 Co-current reactor: FT-IR spectra of (a) monomer TMDS (ATR) and at fixed ϕ_{O_2} (4 sccm) and for varying ϕ_{TMDS}: (b) 5; (c) 10; (d) 20; (e) 40; (f) 80; (g) 120; (h) 160 (sccm). (P_u = 300 W; p = 4.8 hPa; ϕ_{N_2} = 1.8 slpm).

without dioxygen addition [Fig. 10(b)], and deposit with dioxygen addition [Fig. 10(c)]. The deposit without dioxygen addition differs from fused silica by the appearance of bands located at 2904 and 2965 cm^{-1}, which correspond to the symmetric and antisymmetric stretching modes of the methyl groups. The band corresponding to the symmetric stretching mode of R—Si—O—Si—R is not observed. However, for the deposit with oxygen addition, a band at 491 cm^{-1} corresponding to this mode appears clearly. Correlatively, bands are observed at 171, 687, and 786 cm^{-1}, which correspond to C—Si—O bending, Si—C stretching, and Si—C—H bending motions, respectively. At last, bands corresponding to the bending modes of the methyl groups are observed at 1260 and 1408 cm^{-1}.

FT-IR Analysis of Plasma Polymers in the Countercurrent Reactor

Figure 11 shows FT-IR spectra of deposits in the stopping area [Fig. 11(a)] and downstream from the injector inlet [Fig. 11(b)] where only bands assigned to stretching modes of methyl groups (2960 cm^{-1}), Si—C stretching and CH_3 bending modes in Si—$(CH_3)_1$ (1270 cm^{-1}), and Si—O—Si antisymmetric stretching modes (between 1150 and 1010 cm^{-1}) are present.

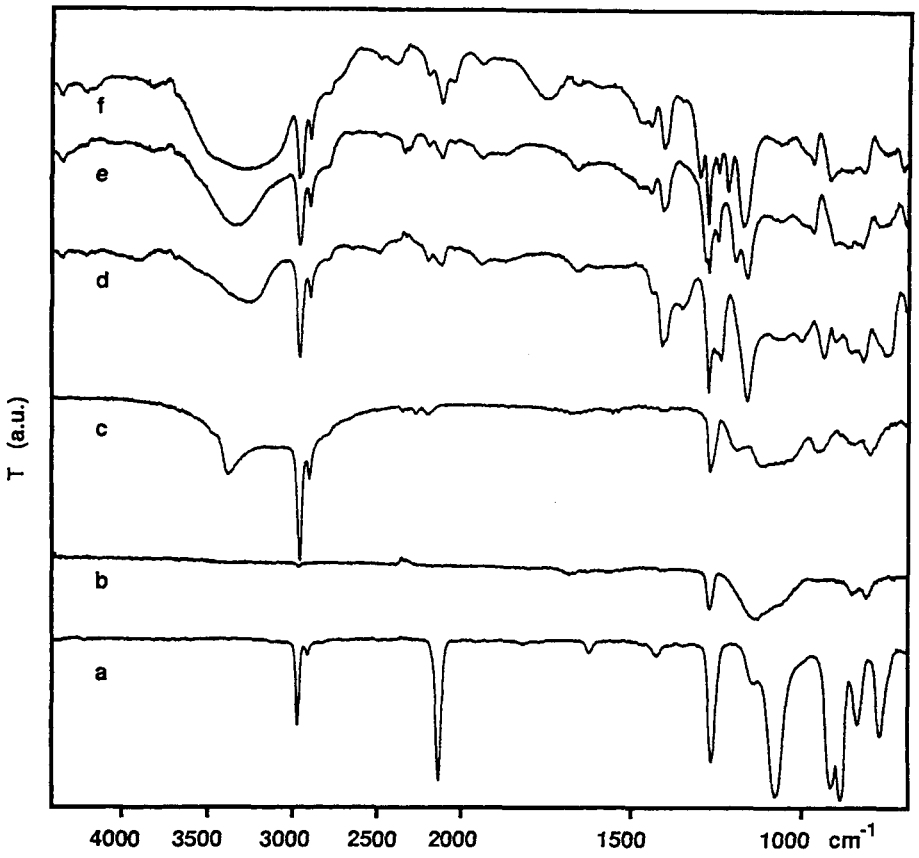

Figure 9 Co-current reactor: FT-IR spectra of (a) monomer TMDS (ATR) and of a deposit at fixed ϕ_{TMDS} (20 sccm) and for varying ϕ_{O_2}: (b) 0; (c) 4; (d) 20; (e) 40; (f) 80 (oil) (sccm) (P_u = 300 W; p = 4.8 hPa; ϕ_{N_2} = 1.8 slpm).

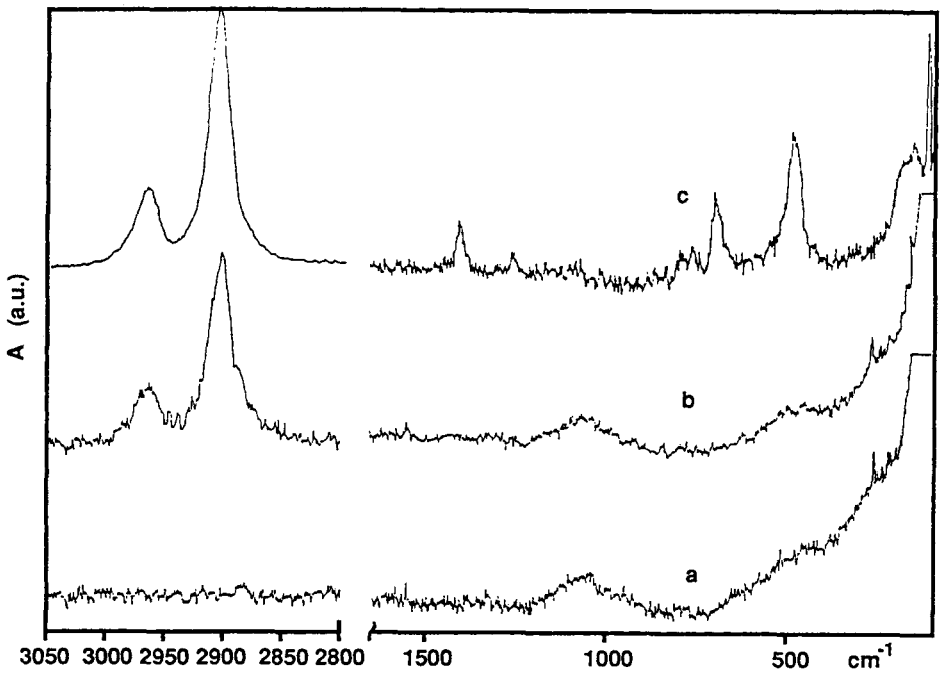

Figure 10 Co-current reactor: Micro-Raman spectra of (a) fused silica and of a deposit at (b) ϕ_{TMDS} = 20, ϕ_{O_2} = 0; (c) ϕ_{TMDS} = 20, ϕ_{O_2} = 20 (sccm) (P_u = 300 W; p = 4.8 hPa; ϕ_{N_2} = 1.8 slpm).

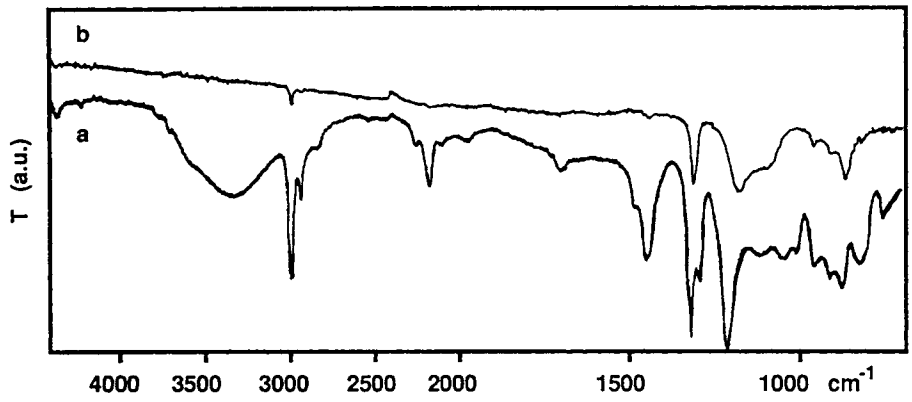

Figure 11 Countercurrent reactor: ϕ_{TMDS} (sccm)/ϕ_{O_2} (sccm) = 120/20: FT-IR spectra of (a) deposit at 10 mm upstream from the injector inlet (stopping area); (b) deposit at 400 mm downstream from the injector inlet (injector inlet: 0 mm) (P_u = 700 W; p = 4.8 hPa; ϕ_{N_2} = 1.8 slpm).

The deposit obtained in the stopping area [Fig. 11(a)] shows a broad absorption band between 3500 and 3300 cm^{-1} due to an overlapping of the OH band in silanol and the NH band in silazane. Methyl absorption bands are drastically more intense (CH stretching mode at 2960 cm^{-1} and CH bending mode at 1410 cm^{-1}). The bands corresponding to Si—C stretching and CH_3 bending modes are more complex and are a mixture of the bands assigned to CH in $Si(CH_3)_1$ (1270 cm^{-1}) and in $Si(CH_3)_3$ (1250 cm^{-1}). The Si–O–Si band is broader and more complex too. The two bands observed at 1170 and 950 cm^{-1} confirm the hypothesis of a silazane Si—NH—Si structure formation in the process with oxygen contribution.

DISCUSSION

The results of the gas phase spectroscopic study[18] and the present spectroscopic analysis allow us to propose successive steps. The first is an initiation step involving a $N(^4S)$ attack in an hydrogen abstraction, which is common for both CRNP–TMDS and CRNP–TMDS–O_2 systems. Propagation steps are closely dependent, in each system, on the interaction mode of the energy carrier like $N_2(A\ ^3\Sigma)$, $N(^4S)$, or its recombination products. In the presence of dioxygen, the situation is quitely complicated by the fact that the kinetics of the reaction between the CRNP and dioxygen is not clear and requires some further experimental and theoretical research.[5] Moreover, in the CRNP–TMDS–O_2 system, an active role of dioxygen in the polymerization processes is given, interpreting more closely the spectacular enhancement of the deposition rate and the chemical deposit structure modification.

$N(^4S)$-Initiated Mechanisms Common to Both CRNP–TMDS and CRNP–TMDS–O_2 Systems

Those mechanisms occur either with or without dioxygen in the reactive media. The first reaction is an initiation step that consists in an hydrogen abstraction by the $N(^4S)$ attack.

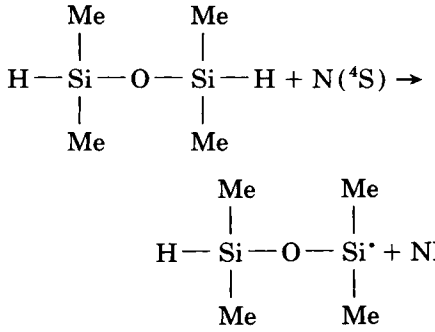

This step can be followed by a second hydrogen abstraction by $N(^4S)$ leading to the diradical formation:

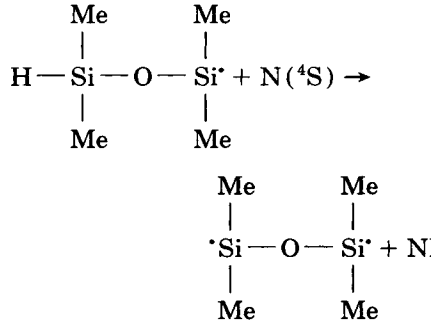

The monoradical or the diradical that originates, respectively, from (1) or from (2) can lead to a fragmentation process by collision with two nitrogen atoms $N(^4S)$. This fragmentation can be reinforced by the inductive effect of the methyl groups:

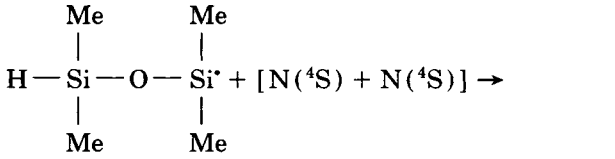

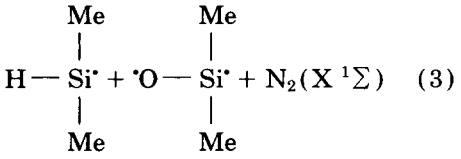

(3)

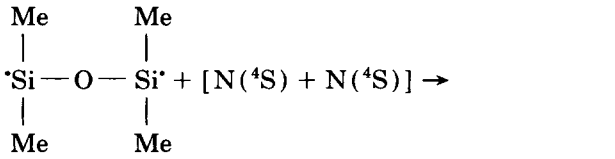

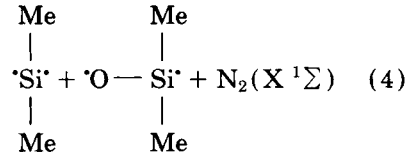

(4)

Each process (3) or (4) is meant to be the global scheme of a probable two-step reaction where two $N(^4S)$ atoms are successfully involved.

The $H-(CH_3)_2Si^{\bullet}$ radical is able to react with $N(^4S)$ by an hydrogen abstraction as follow:

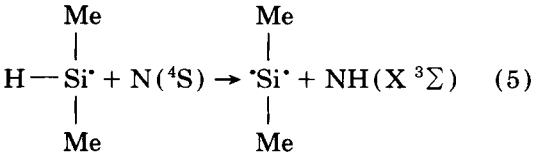

(5)

The main patterns induced by the monomer degradation are:

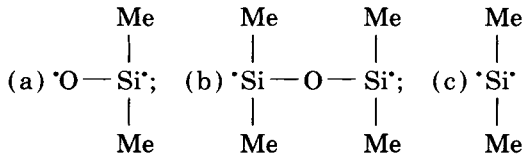

The (a) radical or its isomeric form, the dimethylsilanone $(CH_3)_2Si{=}O$, which is expected to be the main dissociation product of TMDS,[21] is known to be highly reactive by promoting polymerization and by its insertion into other chemical bonds.[22]

Mechanisms in the CRNP–TMDS System

The silicalike structure of the deposit [Fig. 10(b)] implies an efficient methyl removing. It can be achieved by $N_2(A\ ^3\Sigma)$ and/or $N(^4S) + N(^4S)$, which interact with the intermediate radicals (a), (b), and (c), gives successive steps of one methyl abstraction leading mainly to $^{\bullet}O-Si:$, $:Si-O-Si:$ and :Si: radicals.

The probable higher reactivity of $N_2(A\ ^3\Sigma)$ with respect to free radicals, compared to that of $N(^4S)$, balances its much lower concentration. The estimated $N(^4S)$ concentration of about 10^{14} atoms/cm^3 implies, for $N_2(A\ ^3\Sigma)$, a steady-state concentration, with respect of the kinetic of its well-known major creation and destruction processes,[23,24] of about 10^9 molecules/cm^3. The hydrogen abstraction for TMDS, in the initiation step, is more efficient than methyl abstraction for HMDS. A much lower free radical production is expected in the last case. It is confirmed by the poor deposition rate in the CRNP–HMDS system. A conclusion is that methyl abstraction by $N_2(A\ ^3\Sigma)$ requires free radicals to occur.

The deposit shows a highly crosslinked structure that can be understood by the recombination of short and multiradicalar fragments. A more drastic requirement is the existence of a radical with an available oxygen site for creation of the "O" bridge of the silicalike structure. Among (a), (b), and (c) patterns, the only radical that fulfills this point is (a). The (b) Si—O—Si pattern can, hence, be considered as a main source of (a)-type radicals by processes (3) and (4). Indeed, the remaining methyl-abstracted (b)-type radical fits well with the silicalike structure, but its direct deposition requires more methyl abstraction than for the (a)- or (c)-type radicals. It is reasonable to think that (b) does not play an important role in the polymerization process in itself. This remark implies that processes (3) and (4) are very efficient. It can be noted that the small radical polymerization is consistent with the moderate deposition rate observed. The (c) pattern fragmentation is assumed to be the way of production of silicon atoms, in which emission lines have been observed.[18] The other produced radicals, such as CH_3, react rapidly with the CRNP to give diatomic molecules such as CN or CH. The last gaseous products diffuse toward the walls of the reactor and are evacuated by the pumping.

CRNP–TMDS–O_2 System: Mechanisms Induced by Oxygen Adjunction

The significant fact of this dioxygen addition on the deposit structure is the many remaining methyl

groups in $=Si-(CH_3)_2$. Other distinctive features are the intensification of hydrogen-bonded silanol $\equiv Si-OH$ vibration and the surprising selective nitrogen fixation in a silazane $\equiv Si-NH-Si\equiv$ function. It would, *a priori,* appear that dioxygen $O_2(X\,^3\Sigma)$ addition inhibits reaction of such methyl abstraction, but the real situation is rather complicated by efficient gas phase reactions[25] such as:

$$N(^4S) + O_2(X\,^3\Sigma) \rightarrow NO(X\,^2\Pi) + O(^3P) \quad (6)$$

$$N(^4S) + NO(X\,^2\Pi) \rightarrow O(^3P) + N_2(X\,^1\Sigma) \quad (7)$$

The $O(^3P)$ oxygen atoms are known for their reactivity with respect to either hydrogenated molecules or radicals. They are, indeed, in competition with $N(^4S)$ and $N_2(A\,^3\Sigma)$ in the initiation steps and methyl abstraction. The $O(^3P)$-induced hydrogen abstraction leads to OH and H_2O. So, oxygen fixation can occur by the rapid reaction:

$$\equiv Si^{\bullet} + O(^3P) \rightarrow \equiv Si-O^{\bullet} \quad (8)$$

The $\equiv Si-O^{\bullet}$ radicals that originate from (8) are able to participate to polymerization processes in a very efficient manner. It can be noted that these radicals can be formed whatever is the initial radical length. Consequently, (b)- and (c)-type radicals can play an active role on the polymerization processes:

$$\equiv Si-O^{\bullet} + =Si^{\bullet}-O^{\bullet} \rightarrow \equiv Si-O-Si-O^{\bullet} \quad (9)$$

$$\equiv Si-O^{\bullet} + \equiv Si^{\bullet} \rightarrow \equiv Si-O-Si\equiv \quad (10)$$

Reaction (10) can be proposed as a termination step. The probable high OH concentration allows for another termination way such as:

$$\equiv Si^{\bullet} + OH \rightarrow \equiv Si-OH \quad (11)$$

As mentioned above, the gas phase OH density increases with ϕ_{O_2} promoting mainly reaction (11). A consequence is the observation of the intensification of the hydrogen-bonded silanol vibration in the FT-IR spectra (Fig. 9).

The inhibition of reaction of methyl abstraction may originate from the consumption of $N_2(A\,^3\Sigma)$ or its precursors by reactions such as (6) and (7) or reactions[26,27] such as:

$$N_2(A\,^3\Sigma) + O(^3P) \rightarrow N(^4S) + NO^* \quad (12)$$

$$N_2(A\,^3\Sigma \text{ or } B\,^3\Pi) + O_2(X\,^3\Sigma) \rightarrow N_2(X\,^1\Sigma) + 2O(^3P) \quad (13a)$$

$$\rightarrow N_2O + O(^3P) \quad (13b)$$

$$N_2(A\,^3\Sigma) + OH(X\,^2\Pi) \rightarrow N_2(X\,^1\Sigma) + OH(A\,^2\Sigma) \quad (14a)$$

$$\rightarrow N_2(X\,^1\Sigma) + O(^3P) + H(^2S) \quad (14b)$$

These global considerations allow a good understanding of the polysiloxane spectroscopic behavior of the deposit. This model is also in quite good agreement with the spectacular enhancement of V_D.

Oily deposit occurrence, when $\phi_{Tot} = \phi_{O_2} + \phi_{TMDS}$ increases, is well explained by quick OH termination reaction (11) of short chains. The efficient termination leads to the dropping of the crosslinking degree, and then, of the volumic mass of the bulk material. This hypothesis is confirmed by the relative low volumic mass of the oily deposit (1.13 g/cm^3), which is intermediate between the polydimethylsiloxane volumic mass (0.92–0.98 g/cm^3) and the hard film volumic mass (1.34 g/cm^3). The $Si(CH_3)_3$ groups at chain ends are assumed to arise in the reaction of $^{\bullet}CH_3$ on $-\,^{\bullet}Si(CH_3)_2$ or by a rearrangement of the bulk material.

Nitrogen Fixation in the CRNP–TMDS–O_2 System

Nitrogen fixation has been evidenced by FT-IR. Unfortunately, this technique does not allow a quantitative measurement of the N/O ratio in the deposit. This nitrogen fixation is a surprising feature of our results. Indeed, no nitrogen fixation is observed in the deposit from the CRNP–TMDS system. Moreover, the destruction of $\equiv Si-\,^{\bullet}NH$ radicals by reactive species of the CRNP is not very efficient because of its remaining in the tetramethyldisilazane–CRNP assisted polymerization.[28] In our case, the direct NH reaction on $^{\bullet}Si\equiv$ radical is then unrealistic. These considerations and the increase of $Si-NH-Si$ vibration in the FT-IR spectra versus ϕ_{O_2} (Fig. 9) allow us to propose that the nitrogen fixation needs an oxygenated intermediate

to occur. OH appears to be a probable candidate for this nitrogen fixation by the known reaction scheme[29]:

$$\equiv SiCH_3 + O(^3P) \rightarrow \equiv Si-{}^{\bullet}CH_2 + OH \quad (15a)$$

$$\equiv SiCH_3 + OH \rightarrow \equiv Si-{}^{\bullet}CH_2 + H_2O \quad (15b)$$

The $\equiv Si-{}^{\bullet}CH_2$ radical, which originates from (15), can react by the successive processes and promote nitrogen fixation:

$$\equiv Si-{}^{\bullet}CH_2 + N(^4S) \rightarrow \equiv Si-CH_2-N: \quad (16)$$

$$\equiv Si-CH_2-N: + \equiv Si^{\bullet} \rightarrow \equiv Si-CH_2-N^{\bullet}-Si\equiv \quad (17)$$

This last radical can be decomposed, giving $\equiv Si-{}^{\bullet}CH_2$ and $:N-Si\equiv$ radicals.

$\equiv Si-N:$ can react to give silazane function by its recombination with another $\equiv Si^{\bullet}$ radical by the processes:

$$\equiv Si-N: + H \rightarrow \equiv Si-{}^{\bullet}NH \quad (18)$$

$$\equiv Si-{}^{\bullet}NH + \equiv Si^{\bullet} \rightarrow \equiv Si-NH-Si\equiv \quad (19)$$

An interesting feature of the FT-IR spectrum for high ϕ_{O_2} [Fig. 9(f)], is the appearance of an absorption band in the range of 1660–1680 cm^{-1}. This band cannot be easily attributed. The $\diagdown C=N-$ absorption band in $\equiv Si-CH=N-$ group can be proposed by analogy to the $\diagdown C=N-$ absorption band in the chromophore $\varphi-CH=N-R$ (1654 cm^{-1}) and in aliphatic compounds $R-CH=N-R$ (1673 cm^{-1}). Under those conditions, the OH concentration is meant to be important enough to lead to a similar reaction to (15):

$$\equiv Si-{}^{\bullet}CH_2 + OH \rightarrow \equiv Si-:CH + H_2O \quad (20)$$

Nitrogen fixation on the diradical $\equiv SiCH:$ allows a good explanation of the $\diagdown C=N-$ absorption band observed in the FT-IR spectrum:

$$\equiv Si-:CH + N(^4S) \rightarrow \equiv Si-CH=N^{\bullet} \quad (21)$$

Flowing Dependence of Deposit Formation

Experimental results show that the maximal V_D is obtained in the stopping area of the countercurrent reactor where the flows speed is minimized. This characteristic can be interpreted by the very good homogeneity of the reaction zone, which can optimize the radicals collision probability. In this case, the deposit presents a very low superficial energy due to a specific surface structure. This low superficial energy can be assumed by a preferential orientation of apolar methyl groups outside the interface. This particular geometrical distribution is allowed by an efficient piling up of molecular fragments.

The crosslinking of these fragments involves a conformational rearrangement of cumbersome radicals as CH_3 outside of the interface as follow:

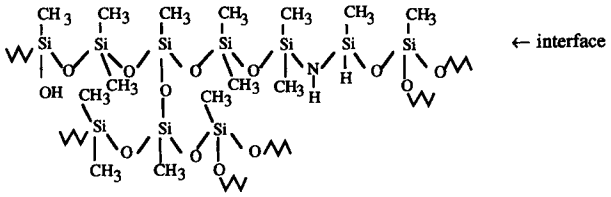

CONCLUSION

Cold remote nitrogen plasma assisted polymerization of siloxanes allows us to obtain polymeric layers. This selective process is only efficient for silane-terminated organosiloxane molecules. V_D are 10 to 100 times higher than in discharge plasma processes with the same compound and for a similar volumic mass range.

For both CRNP-TMDS and CRNP-TMDS-O_2 systems studied, a reactions model has been developped involving a hydrogen abstraction from monomer molecule, followed by formation of a $\equiv Si-O^{\bullet}$ type of radical, which is the major polymerization promoter.

In the binary system, this last radical is mainly produced, after hydrogen abstraction by $N(^4S)$, by the fragmentation of the $Si-O-Si$ pattern induced either by $N_2(A\ ^3\Sigma)$ or $N(^4S)$.

In presence of dioxygen, this fragmentation mechanism is overshadowed by direct oxygen atom fixation on $\equiv Si^{\bullet}$ terminations, whatever the pattern length. The oxygen atoms are provided by oxygenated molecules dissociation products (e.g., O_2, NO, OH, etc.).

Methyl abstraction by $N_2(A\ ^3\Sigma)$ is strongly inhibited by O_2 adjunction. The increase of the radical polymeric fragment length with O_2 adjunction, and consequently of the deposition rate, gives a good explanation to account for the remaining of the methyl groups on the deposit.

An important role of the hydroxyl radical (OH) is suggested in the termination processes and undirect nitrogen fixation.

This model is in quite good agreement with both the silicalike structure of the deposit obtained in the CRNP–TMDS system and the highly hydrocarbonated crosslinked polysiloxane network obtained in the CRNP–TMDS–O_2 system.

It is clear that further investigations are required to corroborate this reactions model. A special effort should be done to support the multiradical intermediates mechanisms, both with spectroscopic diagnostics (laser-induced fluorescence, electron paramagnetic resonance) and mass spectrometry measurements.

REFERENCES

1. H. Yasuda, *Plasma Polymerization,* Academic Press, New York, 1985.
2. H. Yasuda and T. Hsu, *J. Polym. Sci.-Polym. Chem.,* **15,** 81 (1977).
3. M. R. Wertheimer and H. P. Schreiber, *J. Appl. Polym. Sci.,* **26,** 2087 (1981).
4. M. R. Wertheimer, J. E. Klemberg-Sapieha, and H. P. Schreiber, *Thin Solid Films,* **115,** 109 (1984).
5. H. V. Boenig, *Fundamentals in Plasma Chemistry and Technology,* Technomic, Lancaster-Basel, 1988.
6. G. Akovali and N. Dilsiz, *Polym. Eng. Sci.,* **30,** 485 (1990).
7. F. Callebert, O. Dessaux, and P. Goudmand, *10th International Symposium on Plasma Chemistry,* Bochum, **3,** 2.3.3 (1991).
8. F. Callebert, C. Dupret, O. Dessaux, and P. Goudmand, Intern. Pat. Application, WO 92/03591 (1992).
9. O. Dessaux and P. Goudmand, *Congrès International Micro-Ondes et Hautes Fréquences,* Nice, **2,** 57 (1991).
10. G. Akovali and M. Y. Boluk, *Polym. Eng. Sci.,* **21,** 658 (1981).
11. A. M. Wrobel, M. R. Wertheimer, J. Dib, and H. P. Schreiber, *J. Macromol. Sci.-Chem.,* **A14**(3), 321 (1980).
12. A. M. Wrobel, J. E. Klemberg, M. R. Wertheimer, and H. P. Schreiber, *J. Macromol. Sci.-Chem.,* **A15**(2), 197 (1981).
13. E. Radeva, D. Tsankov, K. Bodev, and L. Spassov, *J. Appl. Polym. Sci.,* to appear.
14. G. Akovali, *Polym. Eng. Sci.,* **21,** 662 (1981).
15. K. Kashiwagi, Y. Yoshida, and Y. Muyarama, *Jpn. J. Appl. Phys.,* **30,** 1807 (1991).
16. A. M. Wrobel, M. Kryszewski, and M. Gazicki, *Polymer,* **17,** 678 (1976).
17. G. Moreau, O. Dessaux, and P. Goudmand, *J. Phys. E: Sci. Instrum.,* **16,** 1160 (1983).
18. P. Supiot, F. Callebert, O. Dessaux, and P. Goudmand, *Plasma Chem. Plasma Proc.,* **13**(3), 539 (1993).
19. J. Gnado and P. Dhamelincourt, *J. Raman Spectrosc.,* **24,** 63 (1993).
20. D. R. Anderson, in *Infrared, Raman and Ultra-violet Spectroscopy, Analysis of Silicone,* Wiley-Interscience, New York, 1974.
21. S. Tobita and S. Tajima, *Organic Mass Spectrom.,* **25,** 39 (1990).
22. R. J. Buss, P. Ho, and M. E. Weber, *Plasma Chem. Plasma Proc.,* **13**(1), 61 (1993).
23. J. A. Meyer, D. W. Setser, and W. G. Clark, *J. Chem. Phys.,* **76**(1), 1 (1972).
24. D. E. Shemanski, *J. Chem. Phys.,* **64**(2), 565 (1976).
25. A. N. Wright and C. A. Winkler, *Active Nitrogen,* Academic Press, New York, 1968.
26. M. P. Iannuzzi, J. B. Jeffries, and F. Kaufman, *Chem. Phys. Lett.,* **87**(6), 570 (1982).
27. G. H. Ho and M. F. Golde, *J. Chem. Phys.,* **95**(12), 8866 (1991).
28. C. Jama, J.-D. Quensierre, P. Goudmand, and O. Dessaux, 11th International Symposium on Plasma Chemistry, Loughborough, 1993.
29. R. Atkinson, *Environ. Sci. Technol.,* **25,** 863 (1991).

Received June 10, 1993
Accepted December 2, 1993